

# On the Computational Biomechanics of the Intervertebral Disc



A. P. G. Castro, P. Flores, J. C. P. Claro, António M. G. Completo and J. L. Alves

**Abstract** The intervertebral disc (IVD) is a central piece for spine biomechanics. When the IVD fails, there is a high chance that one is suffering from degenerative disc disease (DDD), which is one of the largest health problems faced worldwide. However, DDD and back pain are also strictly related to the other structures in the spine, such as the vertebral bodies (VBs) or the connecting ligaments. An important amount of experimental and numerical works have studied the spine, focusing on the IVD, the VB or the whole spinal segment, but questions on how degeneration occurs and what causes it are still to be fully answered. This chapter deals with finite element (FE) simulations of the non-degenerated human IVD time-dependent behaviour, using a generic IVD + VB FE model. The outcomes are inside the scope of different sources of experimental and numerical literature data, proving that this model is useful to distinguish between healthy and unhealthy loading levels (shown here as above 600–800 N in activity periods for human spine). In other words, the numerical simulations with this FE model demonstrated potential to mimic the IVD. The biomechanical behaviour of the spine is still dependent on multiple factors, but this increased knowledge on overload levels definitely helps to reduce the risk of DDD and other spine-related diseases to occur.

---

A. P. G. Castro (✉)

IDMEC, Instituto Superior Técnico, University of Lisbon, 1049-001 Lisbon, Portugal  
e-mail: [andre.castro@tecnico.ulisboa.pt](mailto:andre.castro@tecnico.ulisboa.pt)

P. Flores · J. C. P. Claro · J. L. Alves

Department of Mechanical Engineering, University of Minho, 4800-058 Guimarães, Portugal  
e-mail: [pflores@dem.uminho.pt](mailto:pflores@dem.uminho.pt)

J. C. P. Claro

e-mail: [jcpclaro@dem.uminho.pt](mailto:jcpclaro@dem.uminho.pt)

J. L. Alves

e-mail: [jlalves@dem.uminho.pt](mailto:jlalves@dem.uminho.pt)

A. M. G. Completo

Department of Mechanical Engineering, University of Aveiro, 3810-193 Aveiro, Portugal  
e-mail: [completo@ua.pt](mailto:completo@ua.pt)

© Springer Nature Switzerland AG 2020

J. Belinha et al. (eds.), *The Computational Mechanics of Bone Tissue*,  
Lecture Notes in Computational Vision and Biomechanics 35,  
[https://doi.org/10.1007/978-3-030-37541-6\\_9](https://doi.org/10.1007/978-3-030-37541-6_9)

# 1 Introduction

## 1.1 Spine Anatomy

The human spine is a complex system, anchored on an advanced neuromuscular control and consisting of four major zones, with respect to its vertebral bodies (VBs): the neck with the cervical VBs (C1–C7), the thoracic VBs (T1–T12), the lumbar VBs (L1–L5) and the sacral VB (S1). Figure 1 shows a representation of the complete human spine, which is also denominated as vertebral column or backbone.

This is a stable structure, even if highly mobile. The major functions of the spine are weight bearing, allowing motion between upper torso and pelvis and protection of the spinal cord and nerve roots [1, 2]. The functional unit of the spine is the motion segment (MS), composed by one central intervertebral disc (IVD), the two adjacent VBs (with the facets) and the peripheral structures (muscles, ligaments and organ-covering membranes) [3, 4].

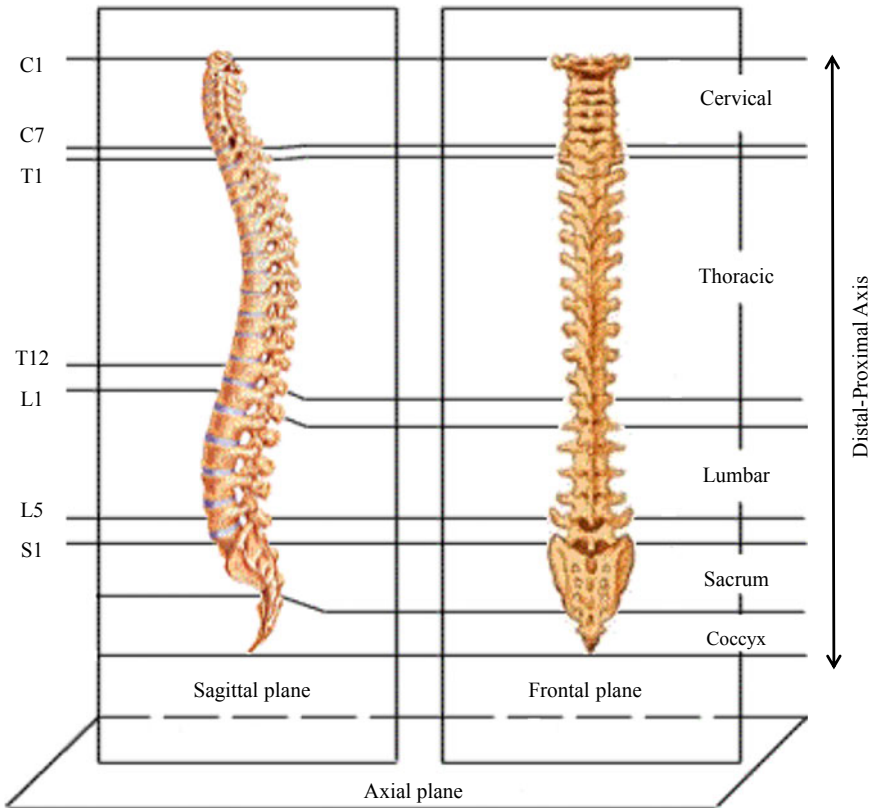
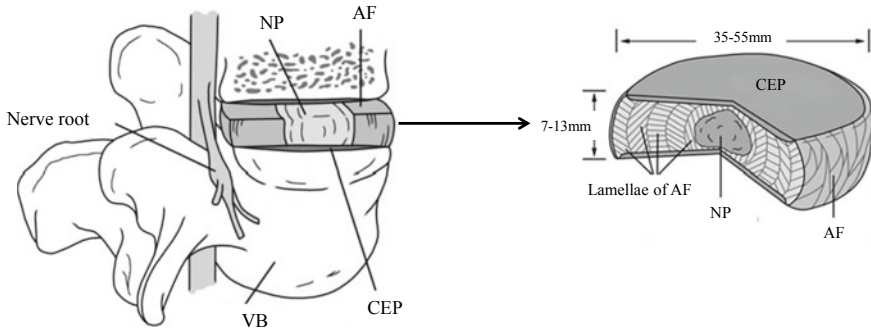


Fig. 1 Complete human spine, in both sagittal and frontal views. Adapted from Noailly [1]



**Fig. 2** Anatomy of an MS, with emphasis on the IVD dimensions. Adapted from Raj [5]

The IVD is an avascular highly inhomogeneous porous structure. Its central structures, the nucleus pulposus (NP) and the annulus fibrosus (AF), are paired structures, vertically limited by the cartilage endplates (CEPs, covering the NP and one-third of the AF) and also the vertebral endplates (VEPs, covering the CEP and two-thirds of the AF). The NP, a jelly structure with embedded fibres, occupies the core of the IVD. Surrounding it, emerge an amount of concentrically arranged fibres supported on a porous matrix, which is the AF [5, 6]. The CEP is a layer of hyaline cartilage that is responsible for most of the nutrients exchange with the VB. Each IVD has approximately 7–13 mm in height and 35–55 mm in diameter (axial plane). If one considers the 23 IVDs stacked, this construct would comprise approximately one-fourth to one-third of the total height of the spine [3, 5, 7]. Figure 2 shows an example of an MS, with the IVD anatomy highlighted.

The VB is substantially stiffer than the IVD. It is a highly porous and vascularized portion of bone tissue, containing both trabecular (TB) and cortical bone (CB) [8]. The VEP is mostly composed by CB. The discrimination between the VEP and the CEP is not always clear, as some authors only refer to the “endplate” and do not separate these two structures [9]. However, the CEP only covers the internal one-third of the extension of the AF, which means that this IVD component is also in direct contact with the VB. From the biomechanical point of view, the interaction between VB and IVD is essential to keep the healthy functioning of the spine, as both components support each other, i.e. the flexibility of the IVD compensates the strength of the VB, and vice versa [10–12].

The regular daily loads acting on the human spine are averagely 200 N during rest (lying prone) and between 600 and 800 N during activity, if one considers the load as independent from the type of solicitation, i.e. all the described activities are equalled to a compressive load. Moderate activities such as level walking, sitting or carrying light objects are within the group of typical daily loading profiles [13]. Harsher activities, such as lifting and carrying heavy objects, may be represented through 1500 or even 2000 N loads [12, 14]. Nevertheless, angular movements are of topmost importance for the spine. Typical moments on the spine for pure flexion

and extension movements are averagely 4–10 Nm, mostly associated with position changes [15, 16].

## ***1.2 Intervertebral Disc Degeneration***

The degeneration of the IVD is firmly associated with the diseases of the spine, particularly low back pain. For many years, a considerable amount of studies have developed efforts to trace the causes and possible solutions for such issue, given that spine problems are a major cause of disability in western societies. Recent reports show that the frequency of these diseases tends to augment every year [17, 18].

The causes for IVD degeneration are not yet fully understood, and the complaints from the patients are also miscellaneous. An assortment of pathways for degeneration may be numbered: it may start with a fracture (or other damage) on the CEP, as a result of abnormal loading or calcification [19]. Proteoglycan loss, first on the CEP and then on the NP, may precipitate degeneration as well [20]. Moreover, it must be highlighted that CEP failure is one of the most important triggers for degenerative disc disease (DDD), as nutrition can be interrupted and so the viability of the IVD cells is compromised. It is thus reinforced that healthy VBs (through the VEPs) are important to keep the nutrients flow, via outer AF, but this pathway is not enough to maintain the integrity of the whole IVD [21].

Ageing is one of the most reported factors for IVD degeneration, i.e. problems such as IVD herniation are associated with senescence of IVD cells. Blood irrigation of the IVD after CEP calcification and cracking is also a collateral effect of ageing, as the IVD is not vascularized. This is another example where the VB is determinant for the healthy functioning of the MS, or how does the VB's condition directly affects the IVD [5, 22, 23]. Nowadays, it is also widely accepted that mechanical stress and inflammatory response are directly connected. At the cellular level, abnormal events (as chronic loading or severe acute efforts) trigger metabolic reactions (which begin with lower nutrients supply) that lead to loss of extracellular matrix integrity, and consequently, losses on IVD functions [19, 23].

Furthermore, the pathway for IVD degeneration may depend on the time of the day: it is recognized that early hours of the day are more suitable to spine injuries, so IVDs become more vulnerable to degeneration if subjected recurrently to efforts during that time. Accumulation of repetitive efforts or, in other words, fatigue has also an important role on promoting the degeneration due to the low metabolic rate presented by the IVD [1, 24, 25].

## ***1.3 Objectives***

The main goal of this chapter is to identify the mechanical loads and mechanical properties of the healthy IVD, accordingly to the state of the art of soft tissue and IVD

constitutive modelling. This objective will be completed with the analysis of several groups of results, namely short creep (computational tests with duration inferior to 3 h, associated with short-term activities) and long creep tests (computational tests with the duration of 48 h, related to the human daily activities).

In order to do so, a custom finite element (FE) solver, V-Biomech<sup>®</sup>, was adopted [26, 27]. This solver includes an innovative biphasic poroelastic formulation particularly developed for soft tissues, such as the IVD, coupled with strain-dependent osmotic swelling behaviour and fibre reinforcement [27–30]. The adoption of this FE solver offers major advantages over commercial software packages, as the rigidity of a proprietary commercial code hampers the freedom of the researcher, when the complexity of the model increases. Given that the researcher has control over the source code, the verifiability of the software is increased.

Numerical simulations on the IVD biomechanical behaviour include comparison with experimental data from various sources [31–33], in order to establish an IVD characteristics framework.

## 2 Materials and Methods

### 2.1 Finite Element Model

The FE simulations were performed with the partial MS FE model shown in Fig. 3, which included L3 and L4 VB (without facets) and the L3–L4 IVD. The most relevant material constitutive modelling and properties of the osmo-poro-hyper-viscoelastic

**Fig. 3** Sagittal cut of the partial human L3–L4 MS FE model, which contains 1892 27-node quadratic hexahedral elements and 16425 nodes. Adapted from Castro et al. [34]

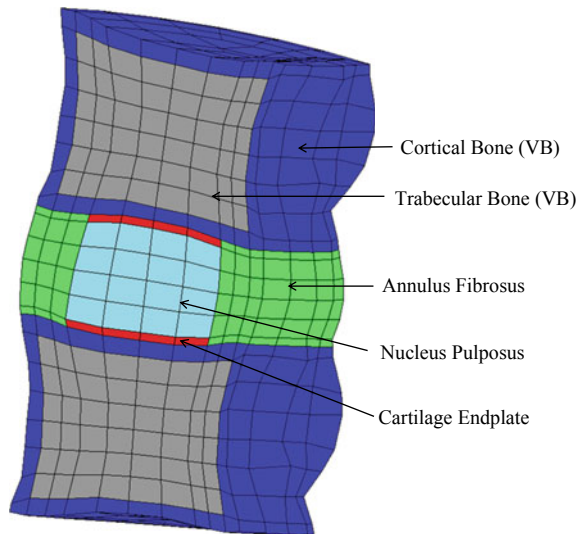


**Table 1** Constitutive models adopted

Isotropy	Mooney-Rivlin	$\bar{W}_{MR}(\bar{\mathbf{C}}) = C_{10}(\bar{I}_1 - 3) + C_{01}(\bar{I}_2 - 3)$
Permeability	van der Voet	$K^*(J) = K_0^* \left( \frac{1-n_{f,0}}{1-n_f} \right)^M = K_0^* J^M$
Anisotropy	Holzzapfel	$\bar{W}_{\text{Holzapfel}}(\bar{\mathbf{C}}, \mathbf{a}_1, \mathbf{a}_2) = \frac{1}{2k_2} \left\{ k_1 \left[ e^{k_2(\bar{I}_4-1)^2} - 1 \right] + k_1 \left[ e^{k_2(\bar{I}_6-1)^2} - 1 \right] \right\}$
Viscoelasticity	Maxwell	$G(t) = 1 + \sum_{n=1}^N a_n \exp\left(-\frac{t}{\tau_n}\right)$
Swelling	Wilson	$\Delta\pi = \pi_{\text{int}} - \pi_{\text{ext}} = \phi_{\text{int}} RT \left( \sqrt{c_F^2 + 4c_{\text{ext}}^2} - 2\phi_{\text{ext}} RT c_{\text{ext}} \right)$
		$c_F = c_{F,0} \frac{n_{f,0}}{n_{f,0}-1+J}$

Adapted from Castro et al. [34]. Please check this reference for further information on each model

and fibre-reinforced model are summarized in Table 1 and Table 2, respectively [27, 34].

Several studies have shown the importance of osmotic swelling behaviour to the IVD biomechanics, namely for the height recovery during rest periods and the maintenance of healthy IDP levels; in agreement, the model was enhanced with Wilson's swelling model [29, 30, 35–37].

Mechanical properties of the AF fibres are assumed to evolve linearly through the axial plane, both in radial and circumferential directions [28, 38]. Fibre angle also varies from  $\pm 23.2^\circ$  at ventral position to  $\pm 46.6^\circ$  at dorsal position [28, 39].

For a more detailed description of the custom FE solver, the biphasic IVD constitutive modelling and MS FE model, the authors would like to refer to Castro et al. [27, 34].

## 2.2 Numerical Simulations

Simulations were divided into short- and long-term creep tests. The works of Heuer et al. [31] and O'Connell et al. [32] were taken into consideration as reference for short-term tests, while the bioreactor data reported by Castro et al. [34] and Paul et al. [40] was considered for the long-term tests. The non-degenerated MS FE model ("FE Nat") was therefore subjected to different load magnitudes and load rates, in order to distinguish between healthy and unhealthy load levels. It must be highlighted that free fluid flow is allowed between the MS components and also on the MS external boundaries at all times so that no artificial barriers are created to the natural IVD behaviour.

In the first test, corresponding to the work of Heuer et al. [31], a uniaxial vertical load of 500 N was applied on the top VB during 5 min (slow loading to allow proper

**Table 2** Material properties of the MS components

		NP	AF	CEP	TB	CB
Isotropy	$C_{10}$ [MPa]	0.15	0.18	1.00	41.67	3846.15
	$C_{01}$ [MPa]	0.03	0.045	0.00	0.00	0.00
Permeability	$K_0^*$ [ $\text{mm}^4 \text{N}^{-1} \text{s}^{-1}$ ]	7.5e-4	7.5e-4	7.5e-3	1.0e-1	1.0e-1
	$M$	8.50	8.50	8.50	18.0	22.0
Anisotropy	$\bar{k}$	–	300.0	–		
	$k_4 = k_6$ [MPa]	–	12.0	–		
Viscoelasticity	$a_1$	1.7	–	–		
	$\tau_1$ [s]	11.765	–	–		
	$a_2$	1.2	–	–		
	$\tau_2$ [s]	1.100	–	–		
	$a_3$	2.0	–	–		
	$\tau_3$ [s]	0.132	–	–		
Swelling	$R$ [ $\text{N mm mmol}^{-1} \text{K}^{-1}$ ]	8.31450	8.31450	–		
	$T$ [K]	298.0	298.0	–		
	$\phi_{\text{int}}$	0.83	0.83	–		
	$\phi_{\text{ext}}$	0.92	0.92	–		
	$C_{\text{ext}}$ [ $\text{mmol} \cdot \text{mm}^{-3}$ ]	0.00015	0.00015	–		
	$C_{F,0}$ [ $\text{mmol} \cdot \text{mm}^{-3}$ ]	0.00030	0.00018	–		
	$n_{f,0}$	0.80	0.70	–		

Isotropic (MS ground substances), permeability, anisotropic (AF fibres), viscoelastic and swelling properties were considered. Adapted from Castro et al. [27]

stabilization of the model) and then held for 15 min. The bottom VB was kept fully constrained. Lateral and sagittal movements were allowed.

For the second test, three stages were considered: (i) a short free swelling preconditioning period (1 h), (ii) a loading period of 2000 N at 1 N/s (in agreement with the experimental test of O’Connell et al. [32] and, finally, (iii) a creep stage (1 h). The global configuration of the boundary conditions was maintained from the previous test.

The third test had two variants: physiological loading and overloading. This involves more complex data and longer-term experiments. Experimental bioreactor data from the loaded disc culture system (LDCS), developed by the Department of Orthopaedic Surgery of VUmc (Amsterdam, The Netherlands), is here considered (Fig. 4). In short, the LDCS maintains the IVDs alive for approximately three weeks after the sacrifice of the animals, under physiological loading conditions. This mechanical stimulation keeps the IVD within its biomechanical and physiological properties, allowing for degeneration or overloading evaluation [40, 42, 43].

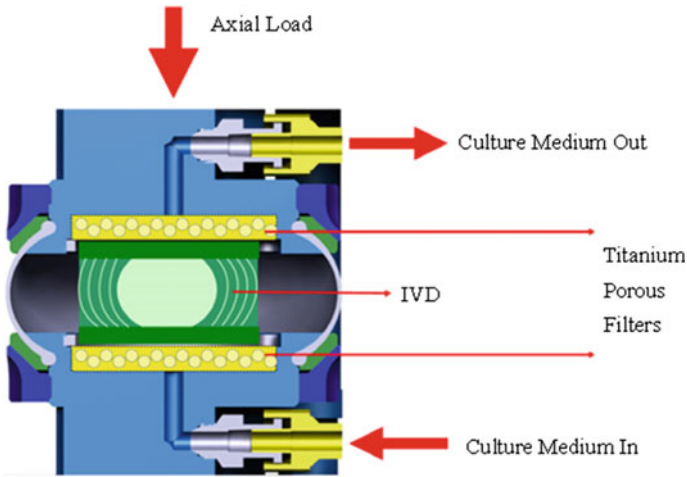


**Fig. 4** Schematic representation of the LCDS system from VUmc. Adapted from Paul et al. [41]

In order to compare the human MS FE model with LDCS data, a normalization factor of four was applied, i.e. the axial cross section of the human IVD is averagely four times larger than the goat IVD, so it was assumed that the loads to be applied on the MS FE model should be four times higher (in magnitude) than the original LDCS loads. In what concerns to height, no normalization was needed, i.e. the IVD FE model has an average height of 12 mm, while the goat IVDs registered an average height of 9 mm. The validity of this approach is supported by the previous reports that human and goat IVDs produce similar internal stresses, regardless of the geometric differences [44–47].

Five goat IVDs were considered for this analysis, having that four were kept under a physiological loading profile (from Goat 1 to Goat 4 Native, abbreviated as “G1–G4 Nat”), and the fifth was overloaded (“G5 Ove”). The physiological loading profile resembles activities such as lying down and walking in goats, equivalent to relaxed standing and unsupported sitting in humans. It consists of a sinusoidal load (1 Hz) of 150 N average and 100 N amplitude for 16 h (activity period), followed by other sinusoidal loads (1 Hz) of 50 N average and 10 N amplitude for 8 h (resting period). It must be highlighted that the transition between the activity and resting periods is performed with 1 h of triangular loading (0.25 Hz) of 200 N average and 100 N amplitude. These were compared with “FE Nat” model.

For “G5 Ove”, the resting period and the transitions between the two major periods were kept, but the activity loading profile consists of a sinusoidal load (1 Hz) of 300 N average and 100 N amplitude for 16 h. This loading profile simulates jumping on a haystack in goats, equivalent to lifting objects in humans. This experiment was compared with the equivalent numerical model, “FE Ove”.

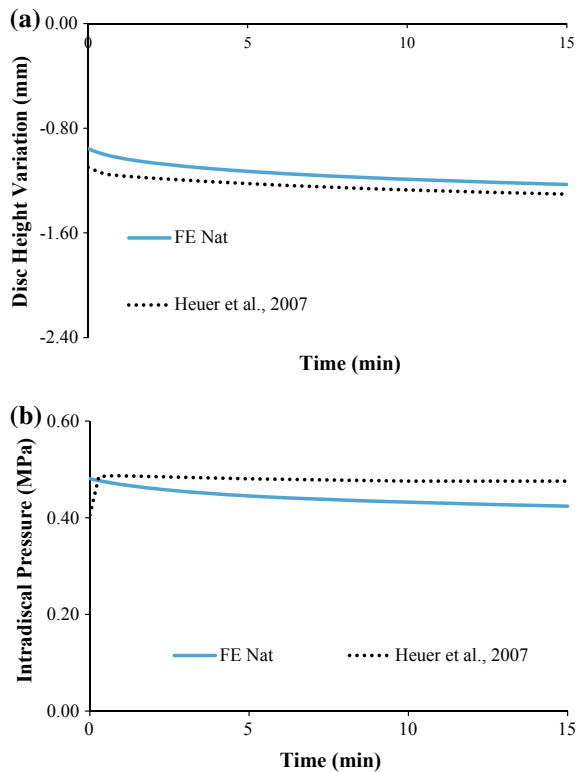


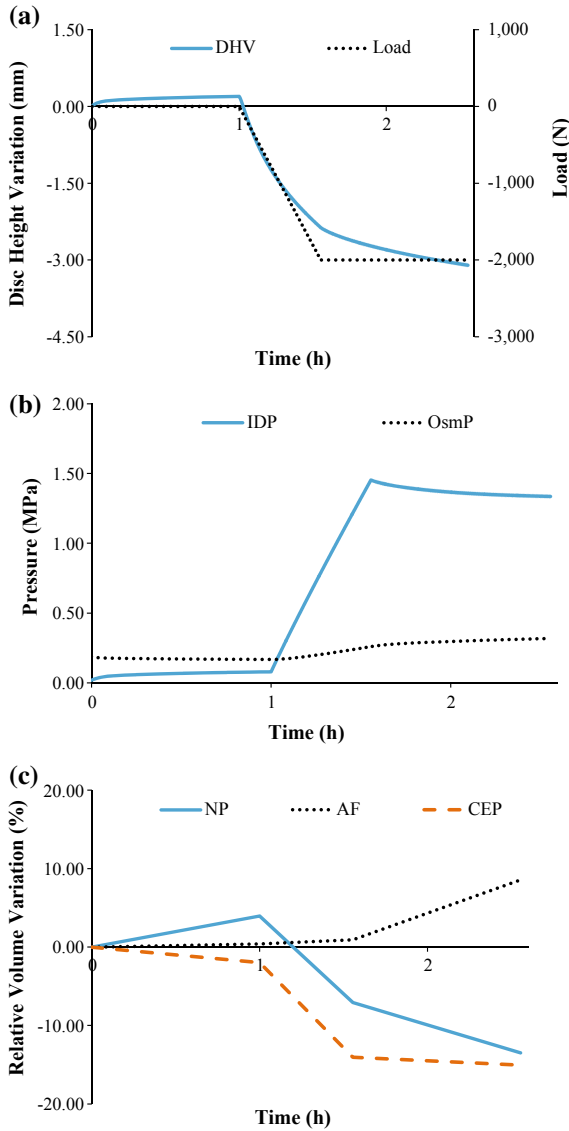
### 3 Results

Figure 5 shows the comparison between experimental results of Heuer et al. [31] and the MS FE model outcomes during a 15-min creep test at 500 N of compression. Figures 6 and 7 show the numerical outcomes of the three-stage short-term creep test based on the work of O’Connell et al. [32]. Figure 8 shows the comparison between LDCS experimental results and the MS FE model outcomes, in both native and overloaded configurations, during two daily cycles.

The assessed parameters, along with the diverse numerical tests, are displacement, hydrostatic pressure and volume variations. Disc height variation (DHV) refers to the height difference calculated between the two VBs at each time. Intradiscal pressure (IDP) is the internal pressure in the IVD tissue, namely in the NP. Osmotic pressure (OsmP) refers to the osmotic swelling pressure, which regulates the IVD osmotic balance and healthy pressure levels. Finally, relative volume variations are calculated with respect to the volume changes occurring during each simulation in the different IVD components.

**Fig. 5** Results of a 15-min creep test at 500 N of compression: **a** DHV; **b** IDP. The experimental work of Heuer et al. [31] is compared with the present MS FE model





**Fig. 6** Three stages loading test with the MS FE model, based on the work of O’Connell et al. [32], involving: (i) a preconditioning period, (ii) a loading period of 2000 N at 1 N/s and, finally, (iii) a creep stage. The following parameters were assessed, considering the full length of the test: **a** DHV versus load; **b** IDP and osmotic pressure of the NP (OsmP); **c** volume variation of NP, AF and CEP

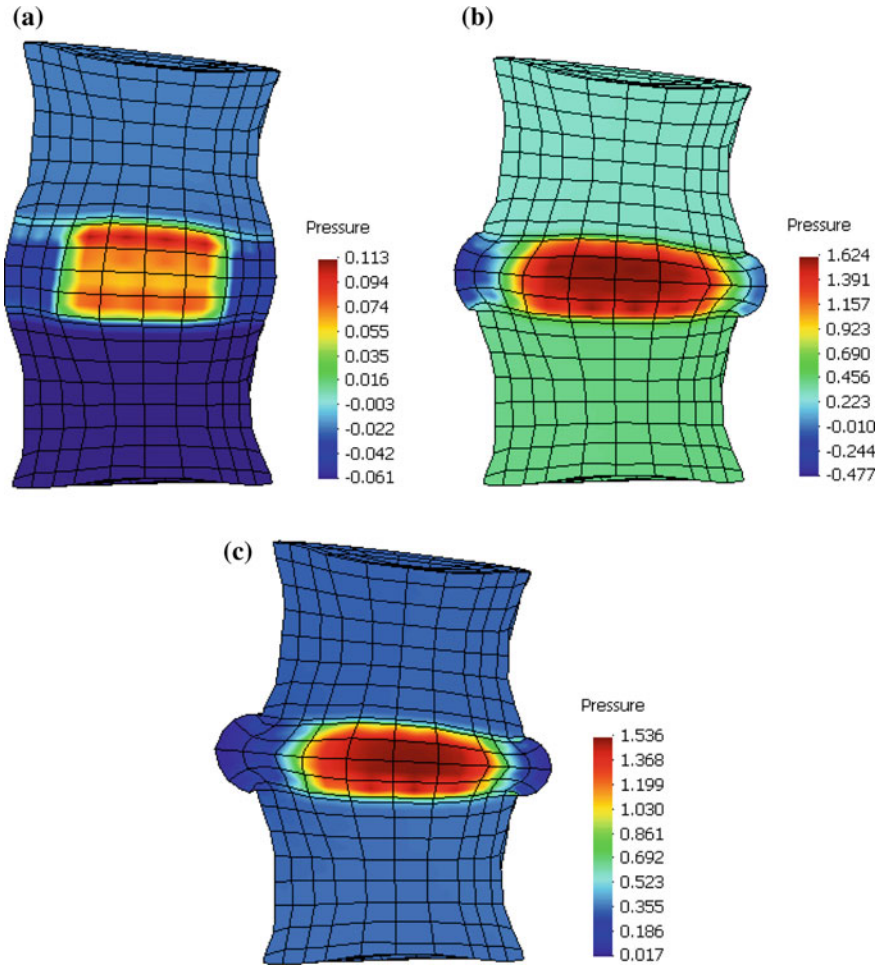


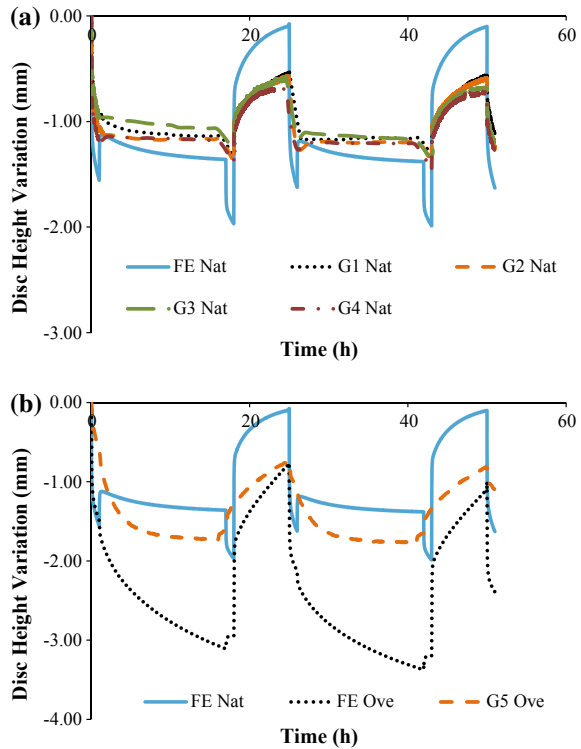
**Fig. 7** Sagittal cuts of the MS FE model, showing the average hydrostatic pressure distribution inside the model at the end of each one of the three stages: **a** after the preconditioning; **b** after the ramp loading; **c** at the end of the test, after the creep phase. The scale is presented on the images (in MPa)

## 4 Discussion

### 4.1 Short Creep Tests

Heuer et al. [31] experimentally measured a range of  $-1.08$  to  $-1.57$  mm of DHV (average of  $-1.32$  mm), at the end of the 15 min with a sustained 500 N load. At the same time, the range of IDP was between 0.36 and 0.52 MPa (average of 0.44 MPa). The correspondent numerical outcomes of the MS FE model are a DHV of  $-1.21$  mm

**Fig. 8** DHV outcomes of the LDCS goat IVDs and correspondent MS FE model for two daily cycles. **a** The four native IVDs compared with the native FE model; **b** the overloaded IVD compared with both native and overloaded FE model



and an IDP of 0.41 MPa (Fig. 5). The differences between the values obtained with the model and those from Heuer et al. [31] are probably related to specimen-to-specimen variability and material properties [48, 49]. Nevertheless, the numerical model showed an overall good agreement with the experimental benchmark, having that the 500 N load allowed the IVD to be kept under physiological conditions [50].

The second short creep test is associated with the experimental test of O’Connell et al. [32], but considering: (i) a preconditioning period of 1 h, (ii) a ramp loading period (compressive uniaxial load) of 2000 N at 1 N/s and (iii) a creep of 1 h. Overall, this test also showed the expected IVD behaviour, with a strong deformation after 1 h of sustained 2000 N (mostly visible in Figs. 6a and 7c). After the ramp loading period, the DHV is 2.55 mm and the IDP is 1.45 MPa (Fig. 6a, b). The comparison of these values with the results of the previous tests indicates that the loading rate influences the stress state of the IVD, but only in what concerns to the pressure measurements. It must be highlighted that the IDP is lower than the OsmP during the first hour of the test (Fig. 6b), due to the free swelling conditions.

The final IDP is 1.32 MPa, which is in agreement with the literature data [33, 51]. The evolution of IDP and OsmP reveals a straight response to the applied load, from the preconditioning to the creep period. The DHV outcomes represent an average reduction of 20% of the initial IVD height, even if the final DHV calculation

was 3.29 mm (or 26% of the initial IVD height). These measurements are in good agreement with the 23% of average axial compression experimentally determined by O'Connell et al. [32], but they probably represent an (almost) irreversible overloading effect [40, 43, 52].

Figure 6c shows that both NP and CEP were losing volume during the loading phases of this test. The final relative volume variation values were  $-13.5\%$  and  $-15.1\%$ , respectively. In contrast, the volume of the AF is increasing throughout the test (8.6% of relative volume variation). This volume increase is due to the fluid flow and pressure gradients within the IVD. The physiological direction of the flow is from the CEP into the inner structures of the IVD, so these volume variation outcomes are most likely in accordance with the literature [53, 54].

Figure 7 confirms that the 2000 N compression is excessive for the MS. Figure 7b shows a clear bulging effect after the ramp loading, even if it does not seem exaggerated. However, after 1 h of sustained 2000 N loading (Fig. 7c), the bulging is visibly unhealthy, as the IVD becomes highly deformed. Nevertheless, the NP still contains most of the pressure, in comparison with the other MS components. The combined analysis of the outcomes shown in Figs. 6 and 7 suggests that the IVD may be able to bear up the ramp loading of 2000 N at 1 N/s, on an (almost) instantaneous or short-term point of view. In that period, the numerical outcomes are inside the range of the results from the work of O'Connell et al. [32], even if the overloading effect is already noticeable. The sustainment of those 2000 N for 1 h seems to be noticeably out of the physiological IVD loading range.

## 4.2 Long Creep Tests

In what concerns to the third and last test, the comparison of the first two daily cycles of the native goat IVDs with the equivalent period of the "FE Nat" model (Fig. 8a) shows that the numerical model is able to reproduce the physiological behaviour of the goat IVDs, particularly during the activity period. The maximum calculated DHV during this period was  $-1.36$  mm, while the average experimental measurement was  $-1.20$  mm. Regarding the resting periods, an important difference is noticed, as the MS FE model is able to regain all the fluid lost during the activity period (DHV close to 0). The goat IVDs do not complete the recovery cycle in the same way, as their average DHV value on the resting period is  $-0.58$  mm.

Nonetheless, these four IVDs maintain the same DHV recovery level from the first to the second daily cycle, which is a sign of no degeneration [23, 34, 40, 55]. In other words, the DHV results indicate no degeneration but incomplete recovery. This fact is probably related to the intrinsic behavioural differences between the goat and human IVDs, namely the specific biomechanical stimuli. The MS FE model helped to understand that the ideal situation is to fully recover the fluid loss during activity on the following resting periods. However, the action of AF fibres may also be limiting the range of DHV, and this limit situation (stretch constraint after

alteration of the loading profile) is not predicted by the MS FE model. This action shall not be considerably different in human and goat spines.

The overloading case is quite different. The DHV calculated from “FE Ove” model is unexpectedly distant from the experimental case (“G5 Ove”, as seen in Fig. 8b), namely during the activity periods. This finding probably indicate that the MS FE model is excessively sensitive to the applied loads, having that the goat IVDs presented a limited range of height variation, as previously mentioned. If these experimental tests were performed *in vivo*, one might argue about the influence of the ligaments, but these structures were removed before the IVDs were tested in the LDCS. Therefore, this noticeable behavioural difference is almost certainly related to the intrinsic biochemical and biomechanical properties of the goat IVDs, counting as well with the contribution of the stretch limit of AF fibres. One may also argue that the human IVDs could have a larger range of DHV, due to their larger cross sections and initial height, but such indication would require further research. However, it must be highlighted that the DHV after recovery is similar for both experimental reference and MS FE model.

## 5 Conclusions

The literature review endorsed the IVD as an inhomogeneous porous tissue. The IVDs provide six degrees of freedom to each spinal MS, serving as central axial cushions for the diverse loading efforts, working together with the VBs to keep spinal healthiness. *In vivo* studies are problematic and potentially harmful, mostly due to the proximity of the spinal canals. Therefore, most of the data on IVD biochemistry and biomechanics comes from *in vitro* studies. Despite the advances in the experimental techniques, which are essential to the description of the biomechanical features of the tissues, the numerical methods are an essential tool to analyse and dissect the IVD behaviour, as they allow unlimited repetitions and complete control over the testing conditions.

In order to achieve valid numerical studies, the IVD was accurately modelled as osmo-hyper-poro-visco-elastic and reinforced with anisotropic fibres. The short and long creep tests have shown that the behaviour of the native MS FE model is aligned with experimental and numerical literature data. It was proved that the MS FE model here developed is able of reproducing experimental studies and also concluded that loads higher than 600–800 N are potentially harmful to the IVD, despite several studies indicating otherwise. The creep response of the MS FE model denoted a clear overload effect when loads of that magnitude were applied, both on displacement and pressure outcomes, i.e. the recovery process of the IVD is impaired for loads higher than 800 N, meaning that higher loads will probably accelerate IVD degeneration.

The analysis of LDCS data showed that the overloading mode caused IVD degeneration, i.e. the overloaded IVD has shown degradation signs, through unrecovered height levels, from the first overloading cycle. Nevertheless, the comparison with the MS FE model was fruitful, also for the physiological situations. Some discrepancies

were noticed between experiments and simulations, probably due to the undisclosed physiological damage-prevention mechanism.

In resume, the numerical simulations with the MS FE model showed its validity and potential to contribute to the understanding of the IVD biomechanics.

## References

1. Noailly J (2009) Model developments for in silico studies of the lumbar spine biomechanics. PhD thesis, Universitat Politècnica de Catalunya, Spain. <http://hdl.handle.net/2117/93381>
2. Niosi CA, Oxland TR (2004) Degenerative mechanics of the lumbar spine. *Spine J.* 4:202–208. <https://doi.org/10.1016/j.spinee.2004.07.013>
3. Ebraheim NA, Hassan A, Lee M, Xu R (2004) Functional anatomy of the lumbar spine. *Semin Pain Med* 2:131–137. <https://doi.org/10.1016/j.spm.2004.08.004>
4. Grumme T, Bittl M (1998) Imaging and therapy of degenerative spine diseases—a neurosurgeon’s view. *Eur J Radiol* 27:235–240
5. Raj P (2008) Intervertebral disc: anatomy physiology pathophysiology treatment. *Pain Pract* 8:18–44. <https://doi.org/10.1111/j.1533-2500.2007.00171.x>
6. Shankar H, Scarlett JA, Abram SE (2009) Anatomy and pathophysiology of intervertebral disc disease. *Tech Reg Anesth Pain Manag* 13:67–75. <https://doi.org/10.1053/j.trap.2009.05.001>
7. Whatley BR, Wen X (2012) Intervertebral disc (IVD): structure, degeneration, repair and regeneration. *Mater Sci Eng C* 32:61–77. <https://doi.org/10.1016/j.msec.2011.10.011>
8. Fields AJ, Lee GL, Keaveny TM (2010) Mechanisms of initial endplate failure in the human vertebral body. *J Biomech* 43:3126–3131. <https://doi.org/10.1016/j.jbiomech.2010.08.002>
9. Swider P, Accadbled F, Laffosse JM, Sales de Gauzy J (2012) Influence of fluid-flow direction on effective permeability of the vertebral end plate: an analytical model. *Comput Methods Biomech Biomed Eng* 15:151–156. <https://doi.org/10.1080/10255842.2010.518960>
10. Adams MA, Dolan P, McNally DS (2009) The internal mechanical functioning of intervertebral discs and articular cartilage, and its relevance to matrix biology. *Matrix Biol* 28:384–389. <https://doi.org/10.1016/j.matbio.2009.06.004>
11. Hussain M, Natarajan RN, An HS, Andersson GBJ (2012) Progressive disc degeneration at C5–C6 segment affects the mechanics between disc heights and posterior facets above and below the degenerated segment: a flexion-extension investigation using a poroelastic C3–T1 finite element model. *Med Eng Phys* 34:552–558. <https://doi.org/10.1016/j.medengphy.2011.08.014>
12. Shirazi-Adl A, Schmidt H, Kingma I (2016) Spine loading and deformation—from loading to recovery. *J Biomech* 49:813–816. <https://doi.org/10.1016/j.jbiomech.2016.02.024>
13. Sato K, Kikuchi S, Yonezawa T (1999) In vivo intradiscal pressure measurement in healthy individuals and in patients with ongoing back problems. *Spine (Phila. Pa. 1976)*. 24:2468–2474
14. Pollintine P, van Tunen MSLM, Luo J, Brown MD, Dolan P, Adams MA (2010) Time-dependent compressive deformation of the ageing spine: relevance to spinal stenosis. *Spine (Phila. Pa. 1976)*. 35:386–394. <https://doi.org/10.1097/BRS.0b013e3181b0ef26>
15. Guan Y, Yoganandan N, Moore J, Pintar FA, Zhang J, Maiman DJ, Laud P (2007) Moment-rotation responses of the human lumbosacral spinal column. *J Biomech* 40:1975–1980. <https://doi.org/10.1016/j.jbiomech.2006.09.027>
16. Rohlmann A, Petersen R, Schwachmeyer V, Graichen F, Bergmann G (2012) Spinal loads during position changes. *Clin Biomech* 27:754–758. <https://doi.org/10.1016/j.clinbiomech.2012.04.006>
17. Stannard JT, Edamura K, Stoker AM, O’Connell GD, Kuroki K, Hung CT, Choma TJ, Cook JL (2016) Development of a whole organ culture model for intervertebral disc disease. *J Orthop Transl* 5:1–8. <https://doi.org/10.1016/j.jot.2015.08.002>

18. Taher F, Essig D, Lebl DR, Hughes AP, Sama AA, Cammisa FP, Girardi FP (2012) Lumbar degenerative disc disease: current and future concepts of diagnosis and management. *Adv Orthop* 2012:970752. <https://doi.org/10.1155/2012/970752>
19. Colombini A, Lombardi G, Corsi MM, Banfi G (2008) Pathophysiology of the human intervertebral disc. *Int J Biochem Cell Biol* 40:837–842. <https://doi.org/10.1016/j.biocel.2007.12.011>
20. Massey CJ, Van Donkelaar CC, Vresilovic E, Zavaliangos A, Marcolongo M (2012) Effects of aging and degeneration on the human intervertebral disc during the diurnal cycle: a finite element study. *J Orthop Res* 30:122–128. <https://doi.org/10.1002/jor.21475>
21. Adams MA, Roughley PJ (2006) What is intervertebral disc degeneration, and what causes it? *Spine (Phila. Pa. 1976)*. 31:2151–2161. <https://doi.org/10.1097/01.brs.0000231761.73859.2c>
22. Hadjipavlou AG, Tzermiadianos MN, Bogduk N, Zindrick MR (2008) The pathophysiology of disc degeneration: a critical review. *J Bone Joint Surg Br* 90:1261–1270. <https://doi.org/10.1302/0301-620X.90B10.20910>
23. Vergroesen P-PA, Kingma I, Emanuel KS, Hoogendoorn RJW, Welting TJ, van Royen BJ, van Dieën JH, Smit TH (2015) Mechanics and biology in intervertebral disc degeneration: a vicious circle. *Osteoarthritis Cartilage* 23:1057–1070. <https://doi.org/10.1016/j.joca.2015.03.028>
24. Martin MD, Boxell CM, Malone DG (2002) Pathophysiology of lumbar disc degeneration: a review of the literature. *Neurosurg Focus* 13:E1. <https://doi.org/10.3171/foc.2002.13.2.2>
25. Qasim M, Natarajan RN, An HS, Andersson GBJ (2012) Initiation and progression of mechanical damage in the intervertebral disc under cyclic loading using continuum damage mechanics methodology: a finite element study. *J Biomech* 45:1934–1940. <https://doi.org/10.1016/j.jbiomech.2012.05.022>
26. Castro APG, Laity P, Shariatzadeh M, Wittkowske C, Holland C, Lacroix D (2016) Combined numerical and experimental biomechanical characterization of soft collagen hydrogel substrate. *J Mater Sci Mater Med* 27:1–9. <https://doi.org/10.1007/s10856-016-5688-3>
27. Castro APG, Wilson W, Huyghe JM, Ito K, Alves JL (2014) Intervertebral disc creep behavior assessment through an open source finite element solver. *J Biomech* 47:297–301. <https://doi.org/10.1016/j.jbiomech.2013.10.014>
28. Cavalcanti C, Correia H, Castro APG, Alves JL (2013) Constitutive modelling of the annulus fibrosus: numerical implementation and numerical analysis. *IEEE 3rd Port Meet Bioeng* 7:3–6. <https://doi.org/10.1109/ENBENG.2013.6518408>
29. Wilson W, van Donkelaar CC, Huyghe JM (2005) A comparison between mechano-electrochemical and biphasic swelling theories for soft hydrated tissues. *J Biomech Eng* 127:158–165. <https://doi.org/10.1115/1.1835361>
30. Wilson W, Van Donkelaar CC, Van Rietbergen B, Huiskes R (2005) A fibril-reinforced poroviscoelastic swelling model for articular cartilage. *J Biomech* 38:1195–1204. <https://doi.org/10.1016/j.jbiomech.2004.07.003>
31. Heuer F, Schmitt H, Schmidt H, Claes L, Wilke HJ (2007) Creep associated changes in intervertebral disc bulging obtained with a laser scanning device. *Clin Biomech* 22:737–744. <https://doi.org/10.1016/j.clinbiomech.2007.04.010>
32. O'Connell GD, Jacobs NT, Sen S, Vresilovic EJ, Elliott DM (2011) Axial creep loading and unloaded recovery of the human intervertebral disc and the effect of degeneration. *J Mech Behav Biomed Mater* 4:933–942. <https://doi.org/10.1016/j.jmbbm.2011.02.002>
33. Wilke H-JJ, Neef P, Caimi M, Hoogland T, Claes LELE (1999) New in vivo measurements of pressures in the intervertebral disc in daily life. *Spine (Phila. Pa. 1976)*. 24:755–762
34. Castro APG, Paul CPL, Detiger SEL, Smit TH, van Royen BJ, Pimenta Claro JC, Mullender MG, Alves JL (2014) Long-term creep behavior of the intervertebral disk: comparison between bioreactor data and numerical results. *Front Bioeng Biotechnol* 2:56. <https://doi.org/10.3389/fbioe.2014.00056>
35. Huyghe JM, Houben GB, Drost MR, van Donkelaar CC (2002) An ionised/non-ionised dual porosity model of intervertebral disc tissue. *Biomech Model Mechanobiol* 2:3–19. <https://doi.org/10.1007/s10237-002-0023-y>



36. Riches PE, Dhillon N, Lotz J, Woods AW, McNally DS (2002) The internal mechanics of the intervertebral disc under cyclic loading. *J Biomech* 35:1263–1271
37. Schroeder Y, Huyghe JM, Van Donkelaar CC, Ito K (2010) A biochemical/biophysical 3D FE intervertebral disc model. *Biomech Model Mechanobiol* 9:641–650. <https://doi.org/10.1007/s10237-010-0203-0>
38. Eberlein R, Holzapfel GA, Schulze-Bauer CAJ (2001) An anisotropic model for annulus tissue and enhanced finite element analyses of intact lumbar disc bodies. *Comput Methods Biomech Biomed Eng* 4:209–229. <https://doi.org/10.1080/10255840108908005>
39. Holzapfel GA, Schulze-Bauer CAJ, Feigl G, Regitnig P (2005) Single lamellar mechanics of the human lumbar annulus fibrosus. *Biomech Model Mechanobiol* 3:125–140. <https://doi.org/10.1007/s10237-004-0053-8>
40. Paul CPL, Schoorl T, Zuiderbaan HA, Zandieh Doulabi B, van der Veen AJ, van de Ven PM, Smit TH, van Royen BJ, Helder MN, Mullender MG (2013) Dynamic and static overloading induce early degenerative processes in caprine lumbar intervertebral discs. *PLoS One* 8. <https://doi.org/10.1371/journal.pone.0062411>
41. Paul CPL, Zuiderbaan HA, Zandieh Doulabi B, van der Veen AJ, van de Ven PM, Smit TH, Helder MN, van Royen BJ, Mullender MG (2012) Simulated-physiological loading conditions preserve biological and mechanical properties of caprine lumbar intervertebral discs in EX vivo culture. *PLoS ONE* 7:29–34. <https://doi.org/10.1371/journal.pone.0033147>
42. Detiger S, de Bakker J, Emanuel K, Schmitz M, Vergroesen P, van der Veen A, Mazel C, Smit T (2015). Translational challenges for the development of a novel nucleus pulposus substitute: experimental results from biomechanical and in vivo studies. *J Biomater Appl* 0:1–12. <https://doi.org/10.1177/0885328215611946>
43. Vergroesen PPA, Van Der Veen AJ, Van Royen BJ, Kingma I, Smit TH (2014) Intradiscal pressure depends on recent loading and correlates with disc height and compressive stiffness. *Eur Spine J* 23:2359–2368. <https://doi.org/10.1007/s00586-014-3450-4>
44. Alini M, Eisenstein SM, Ito K, Little C, Kettler AA, Masuda K, Melrose J, Ralphs J, Stokes I, Wilke HJ (2008) Are animal models useful for studying human disc disorders/degeneration? *Eur Spine J* 17:2–19. <https://doi.org/10.1007/s00586-007-0414-y>
45. Ayotte DC, Ito K, Tepic S (2001) Direction-dependent resistance to flow in the endplate of the intervertebral disc: an ex vivo study. *J Orthop Res* 19:1073–1077. [https://doi.org/10.1016/S0736-0266\(01\)00038-9](https://doi.org/10.1016/S0736-0266(01)00038-9)
46. Hoogendoorn RJW, Helder MN, Kroeze RJ, Bank RA, Smit TH, Wuisman PIJM (2008) Reproducible long-term disc degeneration in a large animal model. *Spine (Phila. Pa. 1976)*. 33:949–954. <https://doi.org/10.1097/BRS.0b013e31816c90f0>
47. Schmidt H, Reitmaier S (2012) Is the ovine intervertebral disc a small human one? A finite element model study. *J Mech Behav Biomed Mater* 17:229–241. <https://doi.org/10.1016/j.jmbbm.2012.09.010>
48. Johannessen W, Elliott DM (2005) Effects of degeneration on the biphasic material properties of human nucleus pulposus in confined compression. *Spine (Phila. Pa. 1976)*. 30:E724–E729. <https://doi.org/10.1097/01.brs.0000192236.92867.15>
49. Périé D, Korda D, Iatridis JC (2005) Confined compression experiments on bovine nucleus pulposus and annulus fibrosus: sensitivity of the experiment in the determination of compressive modulus and hydraulic permeability. *J Biomech* 38:2164–2171. <https://doi.org/10.1016/j.jbiomech.2004.10.002>
50. Araujo ARG, Peixinho N, Pinho A, Claro JCP (2015) The intradiscal failure pressure on porcine lumbar intervertebral discs: an experimental approach. *Mech Sci* 6:255–263. <https://doi.org/10.5194/ms-6-255-2015>
51. Bashkuev M, Vergroesen PPA, Dreischarf M, Schilling C, van der Veen AJ, Schmidt H, Kingma I (2016) Intradiscal pressure measurements: a challenge or a routine? *J Biomech* 49:864–868. <https://doi.org/10.1016/j.jbiomech.2015.11.011>
52. Araujo ARG, Peixinho N, Pinho ACM, Claro JCP (2014) A novel methodology to assess the relaxation rate of the intervertebral disc by increments on intradiscal pressure. *Appl Mech Mater* 664:379–383. <https://doi.org/10.4028/www.scientific.net/AMM.664.379>

53. Ferguson SJ, Ito K, Nolte LP (2004) Fluid flow and convective transport of solutes within the intervertebral disc. *J Biomech* 37:213–221. [https://doi.org/10.1016/S0021-9290\(03\)00250-1](https://doi.org/10.1016/S0021-9290(03)00250-1)
54. Schmidt H, Schilling C, Reyna ALP, Shirazi-Adl A, Dreischarf M (2016) Fluid-flow dependent response of intervertebral discs under cyclic loading: on the role of specimen preparation and preconditioning. *J Biomech* 49:846–856. <https://doi.org/10.1016/j.jbiomech.2015.10.029>
55. Lai A, Moon A, Purmessur D, Skovrlj B, Winkelstein BA, Cho SK, Hecht AC, Iatridis JC (2015) Assessment of functional and behavioral changes sensitive to painful disc degeneration. *J Orthop Res* 33:755–764. <https://doi.org/10.1002/jor.22833>